

# Electronic and vibrational structure of a gold- and lithium-related center in silicon

Per Tidlund and Mats Kleverman

*Solid State Physics, Department of Physics, University of Lund, Box 118, S-221 00 Lund, Sweden*

(Received 27 February 1998)

The electronic and vibrational properties of a gold- and lithium-related center in silicon have been investigated by Fourier-transform spectroscopy in conjunction with uniaxial stress and magnetic field. The excitation spectrum shows close similarity to the previously studied gold-pair center in that it consists of zero-phonon lines followed by several relatively sharp phonon replicas. Transitions to three different series were observed and in all cases phonon energies of about 59 and 47  $\text{cm}^{-1}$  were deduced for the final and initial stages of the transitions, respectively. A Huang-Rhys factor of about 5.7 was determined. In addition to the low-temperature transitions from the initial-state phonon ground state, transitions from the first and the second excited phonon states were observed at higher sample temperatures. Uniaxial stress experiments reveal trigonal symmetry for the center and show that the initial as well as the final electronic states are orbital singlets. Zeeman experiment shows that the center is nonparamagnetic. It is suggested that the center consists of two nearest-neighbor substitutional gold atoms and an unknown number of interstitial Li ions. [S0163-1829(98)06831-3]

## I. INTRODUCTION

The electronic structure of the isolated substitutional gold center and other gold-related centers in silicon have previously been studied in some detail by employing excitation spectroscopy.<sup>1-5</sup> The reason for this interest is the role the isolated substitutional gold center has been recognized to play in the general understanding of the electronic structure of defects as well as its technological importance.<sup>3</sup>

In gold-doped silicon several different excitation spectra have previously been observed. Transitions to the shallow acceptor and donor states have been revealed for the well-known single substitutional gold center<sup>1,2</sup> with a donor and an acceptor level at  $E_V+0.35$  and  $E_V+0.67$  eV, respectively. The dominating excitation spectrum in the Au samples has, however, been attributed to transitions at the trigonal gold-pair center  $\text{Au}_2$ .<sup>5</sup> This spectrum consists of several zero-phonon lines followed by relatively sharp phonon replicas. Phonon energies of about 119.8 and 105.7  $\text{cm}^{-1}$  were found for the neutral and negatively charged states, respectively. A Huang-Rhys factor of about  $1.4 \pm 0.1$  was determined for the neutral charge state.

Yet another gold-related center with a spectral structure similar to that observed for the  $\text{Au}_2$  center (a zero-phonon line together with several phonon replicas) has tentatively been assigned to a complex consisting of the  $\text{Au}_2$  center and iron on a nearby interstitial site, i.e., a  $\text{Au}_2$ -Fe complex.<sup>4</sup> A phonon energy of 57.4  $\text{cm}^{-1}$  and a Huang-Rhys factor of about unity were deduced for this center.

In this paper we discuss the electronic and vibrational structure of an excitation spectrum observed in silicon that has been diffused with both gold and lithium. The spectrum shows a close resemblance to spectra observed previously for the  $\text{Au}_2$  and the  $\text{Au}_2$ -Fe centers in that numerous intense and relatively sharp phonon replicas are observed for several zero-phonon lines. Due to overlap between different series, however, only one zero-phonon line was directly observed. The electronic structure has been investigated by uniaxial stress spectroscopy and a trigonal symmetry was found for

the center that is tentatively assigned as a  $\text{Au}_2$ -Li complex.

## II. EXPERIMENTAL DETAILS

The samples were prepared from *n*-doped floating zone silicon with a resistivity of 1000  $\Omega$  cm. After standard polishing and cleaning procedures, the gold doping was performed by solid-state diffusion. A gold layer with a thickness of approximately 1000  $\text{\AA}$  was evaporated onto one sample surface. The samples were introduced into quartz ampoules, which were evacuated and sealed. A heat treatment at about 1250  $^\circ\text{C}$  for 24 h was followed by a rapid quench to room temperature in ethylene glycol. After cleaning, the sample was introduced into another quartz ampoule with one side of the sample coated by a thin layer of lithium. After evacuation, a heat treatment at about 1100  $^\circ\text{C}$  for 30 min was carried out, which was ended by a rapid quench to room temperature. The samples were then polished for good optical surfaces. Samples prepared in this way are referred to below as Au-Li samples.

The transmission spectra were obtained using a Bomem DA 3.01+ Fourier transform spectrometer equipped with a liquid- $N_2$ -cooled InSb detector. A wire grid polarizer on a  $\text{CaF}_2$  substrate was used in the polarization experiments.

## III. RESULTS AND DISCUSSION

### A. Zero-stress results

A typical excitation spectrum observed for the Au-Li samples is shown in Fig. 1 for two different sample temperatures. Although other sets of lines are observed, the spectrum in Fig. 1 has the highest intensity and dominates. The appearance of this Au- and Li-related spectrum was always connected with a decrease in the intensity of all other Au-related spectra, i.e., those for the Au donor, the Au acceptor, and the  $\text{Au}_2$  center. It is interesting to note that the largest decrease was always observed for the Au-pair lines, suggest-

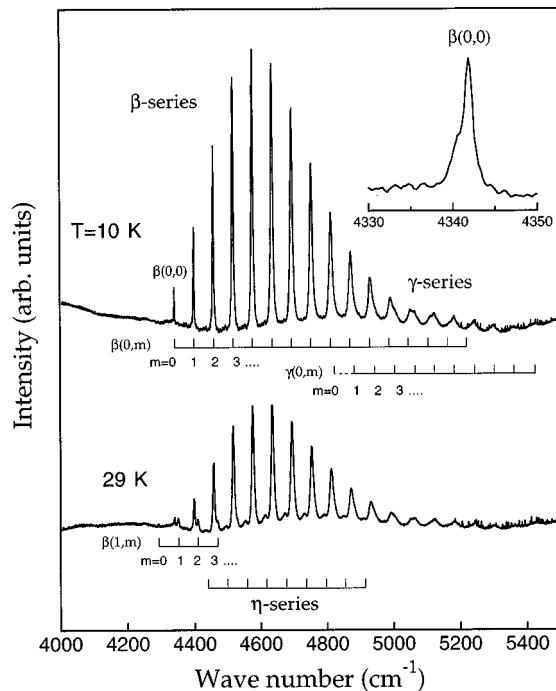


FIG. 1. Transmission spectra of silicon codoped with Li and Au silicon measured at  $T=10$  and  $29$  K.

ing that the Au-Li center is related to  $Au_2$ , i.e., a complex involving interstitial Li and the  $Au_2$  center. Interstitial Li in silicon gives rise to a shallow donor center. It may therefore be expected that the excess Li, which is not complexed with Au or other impurities and defects, raises the Fermi level towards the conduction-band minimum. The decrease in the intensity observed for the Au centers may therefore, at least partly, be caused by changes in the Fermi level position due to incorporation of Li into the samples. It is thus difficult to judge which of the different effects dominates and causes the observed decrease in the intensity of the Au centers and for the  $Au_2$  center in particular.

The Au-Li spectrum consists of several zero-phonon lines (only directly observed for one series) followed by several phonon replicas. The spectrum is thus in many respects similar to those observed for the  $Au_2$  and  $Au_2Fe$  centers. It is instructive to compare the spectral features observed for Au- and Au-Li-doped samples, on the one hand, with those observed for Pt- and Pt-Li-doped silicon, on the other hand. In silicon, the single substitutional Au and Pt centers have similar electronic structure and one would therefore expect that Pt-pair centers are as easily formed at higher diffusion temperatures as has been demonstrated to be the case for Au pairs in Au-doped silicon. This is not the case, however, since no spectral features similar to the  $Au_2$  spectrum have been observed for Pt-doped silicon. This indicates that the formation of substitutional Pt-pair centers  $Pt_2$  is less probable. Accordingly, if no or only a small number of  $Pt_2$  centers are present in the samples there is no reason to expect such a high concentration of  $Pt_2$ -Li complexes that is needed for an optical detection of the centers. Interestingly, no spectrum similar to the one shown in Fig. 1 has so far been detected in our Pt-Li silicon samples.<sup>6</sup> This provides further evidence that the Au-Li center is associated with the  $Au_2$  center.

At  $T=10$  K, a series of relatively sharp lines is detected and is labeled as the  $\beta$  series in Fig. 1. The zero-phonon line is labeled  $\beta(0,0)$ . A closer inspection reveals an additional series, the  $\gamma$  series, which has a considerably lower intensity than the  $\beta$  series. The  $\gamma$  lines appear as weak additional features superimposed on the  $\beta$ -series lines at higher frequency. The  $\gamma$ -series zero-phonon line and the lower phonon replicas have not been directly observed due to their low intensity (see further below). The lines in the two series are labeled  $\beta(n,m)$  and  $\gamma(n,m)$ , where  $n$  and  $m$  are the phonon quantum number for the initial and final states, respectively. At this low temperature (10 K) only the lowest vibrational state in the initial state of the transitions is expected to be significantly populated (see below). About 16 phonon replicas, which all have a phonon energy of about  $\hbar\omega_f = 58.7$   $cm^{-1}$ , are easily revealed for the  $\beta$  series. The anharmonicity in the final state is small since the energy spacing between consecutive phonon replicas is, within experimental error, constant. A closer inspection shows that the  $\beta$ -series zero-phonon line  $\beta(0,0)$  is split into two nearby lines at 4340.7 and 4341.8  $cm^{-1}$ . The doublet has only partly been resolved as is seen in the inset in Fig. 1. We have studied this doublet in some detail at different temperatures in order to reveal any thermalization effects between the lines. No thermalization was observed, which indicates that the origin of the doublet structure is to be found in the final state of the transitions. This doublet structure could not be observed for any of the phonon replicas due to their larger half-widths.

Additional series of excitation lines are observed when higher vibrational levels in the initial state becomes thermally populated. This is clearly demonstrated by comparing the 10- and the 29-K spectra in Fig. 1. In the case of the  $\beta$  series, a series of four lines close to the  $\beta(0,m)$  zero-phonon lines is clearly revealed in the 29-K spectrum. They are due to transitions from the thermally populated first excited phonon level in the initial state. This series is accordingly labeled  $\beta(1,m)$  and a simple analysis based on energy difference between lines having the same final vibrational state in the  $\beta(0,m)$  and  $\beta(1,m)$  series results in a phonon energy of about  $\hbar\omega_i = 47$   $cm^{-1}$  for the initial state. It is interesting to note that this energy is substantially smaller than the one of about 58.7  $cm^{-1}$  deduced for the final state.

In order to add further proof to our results above, the relative intensity for lines in the  $\beta$  series originating from the lowest and first excited phonon states in the initial state was measured for different temperatures. In this way the energy separation between the two lowest phonon states was found to be about 51  $cm^{-1}$ , which compares favorably with the value of 47  $cm^{-1}$  found for  $\hbar\omega_i$  previously.

Both phonons are resonant with the band phonon continuum. The fact that the lines are relatively narrow indicates that the interaction between the discrete phonon states and the continuum is weak. The vibrational modes are therefore, in a first approximation, localized at the defect and directly related to vibrations of the defect constituents.

The difference in the phonon energy in the initial and the final state implies different force constants for the two states. The assumption that the vibrational modes effective mass is the same for the two states results in a final-state force constant that is about 60% larger than the one for the initial

state. This difference may be due to a substantially altered bonding scheme for the two states. In the case of the  $\text{Au}_2$  center, the phonon energy for the negative charge state was found to be slightly smaller than that for the neutral charge state.<sup>5</sup> The difference was interpreted as a mode softening caused by a higher occupancy in an antibonding state for the negatively charged center than for the neutral center.

As is readily seen in Fig. 1, yet another series, the  $\eta$  series, is observed at  $T=29$  K. This series seems already to be weakly detected at 10 K and it is believed to originate from thermal population of an excited electronic state. The relative intensity of the various  $\eta$  lines could only be measured with a substantial uncertainty, which, unfortunately, made it impossible to identify which replica corresponds to a particular final phonon state.

The spectra in Fig. 1 indicate a linear electron-phonon coupling, i.e., a coupling term that is linear in the vibrational coordinate. Furthermore, as will be shown below, the uniaxial stress measurements reveal that the optical transitions take place between two orbitally nondegenerate electronic states [when disregarding the doublet structure observed for the  $\beta(0,0)$  line]. In a harmonic approximation, the intensity for transitions from the initial electronic state  $i$  and phonon state  $n$  to the final electronic state  $f$  and phonon state  $m$  is then approximately given by

$$I_{i \rightarrow f}(E) = I_0 A v_n \sum_m |\langle \chi_f(m) | \chi_i(n) \rangle|^2 \delta(E_{f,m} - E_{i,n} - E), \quad (1)$$

where  $A v_n$  indicates the thermal average over the initial vibrational states  $n$ .<sup>7</sup>  $E_{f,m}$  is the energy of the  $m$ th vibrational state when the center is in the electronic final state  $f$  and similarly for the initial state.  $\chi_i(n)$  and  $\chi_f(m)$  are harmonic-oscillator wave functions for the initial and final states, respectively. An explicit analytical expression in closed form may only be obtained when the harmonic oscillators in the initial and final states have the same phonon energy.<sup>7</sup> This is obviously not the case for the Au-Li center and we have therefore numerically calculated the relative intensities for the various lines at different temperatures using a Huang-Rhys factor  $S=5.7$  and the phonon energies  $\hbar\omega_i=47$   $\text{cm}^{-1}$  and  $\hbar\omega_f=58.7$   $\text{cm}^{-1}$  for the initial and final states respectively.

The calculated relative intensity for the  $\beta$  lines at 10 K [the  $\beta(0,m)$  series] is presented as bars in Fig. 2 and is compared to the corresponding experimental integrated intensity. At this low temperature only the phonon ground state is populated in the initial state of the transitions. The intensity for both partners making up the  $\beta(0,0)$  line was added together in the integrated intensity. This procedure is reasonable since the two partners only are partially resolved for the  $\beta(0,0)$  line and impossible to separate for the phonon replicas. As is readily seen, the calculated line shape and the integrated intensity for the experimental lines are in excellent agreement.

The  $\gamma$ -series spectral features are superimposed on the  $\beta$ -series higher phonon replicas, which made it difficult to directly observe the  $\gamma$  zero-phonon line as well as to deduce the relative intensity accurately for the various lines. Using the same Huang-Rhys factor as for the  $\beta$  series and the same

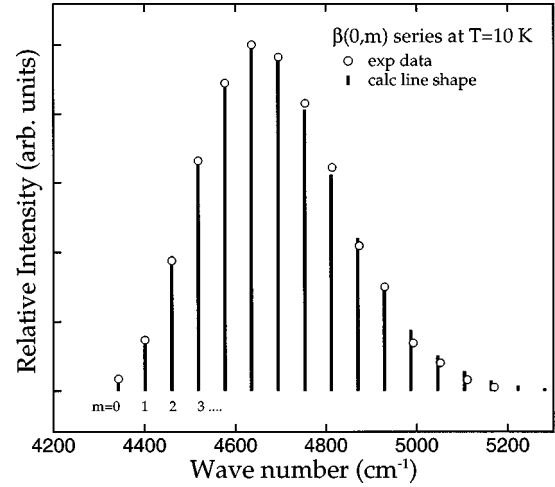


FIG. 2. Calculated relative intensity for the  $\beta(0,m)$  series at  $T=10$  K (bars) and compared to the experimental integrated intensity ( $\circ$ ). The Huang-Rhys factor was  $S=5.7$  and the phonon energies  $\hbar\omega_i=47$   $\text{cm}^{-1}$  and  $\hbar\omega_f=58.7$   $\text{cm}^{-1}$  were used in the initial and final states of the transitions, respectively. See the text for details.

phonon energies, the calculated intensities for the  $\gamma$  series are shown in Fig. 3 and compared to the experimental data. The fit to the experimental points is acceptable when taking into account the difficulty to accurately determining the experimental intensities in general and for the  $\gamma(0,3)$  line in particular (see Fig. 1). Nevertheless, our identification of the phonon replicas seems to be appropriate and the fit enables the energy position for the  $\gamma(0,m)$  series zero-phonon line to be determined to be about  $4823.3$   $\text{cm}^{-1}$ .

We have also carried out numerical calculations of the line shapes expected for  $T=29$  K. The results for three  $\beta$  series as well as the corresponding experimental values for the integrated intensity are presented in Fig. 4. Transitions from the  $n=0, 1$ , and  $2$  initial phonon states for the  $\beta$  series [labeled  $\beta(0,m)$ ,  $\beta(1,m)$ , and  $\beta(2,m)$ , respectively] are observed. For the  $\beta(0,m)$  series, the agreement with experimental data is excellent for the low-phonon replicas, while it is less satisfactory for the higher-phonon replicas. This poor

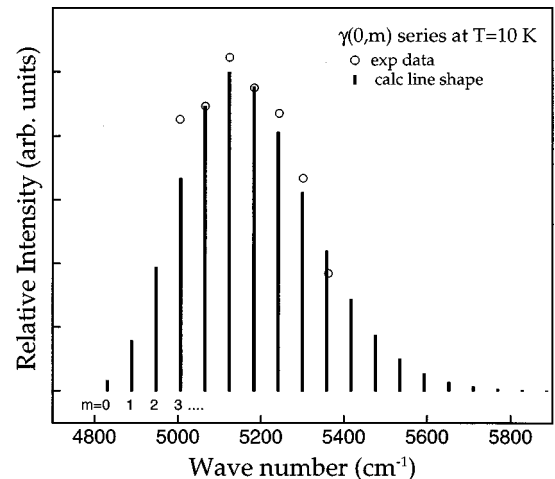


FIG. 3. Calculated relative intensity for the  $\gamma(0,m)$  series at  $T=10$  K (bars) and compared to the experimental integrated intensity ( $\circ$ ). See Fig. 2 and the text for additional details.

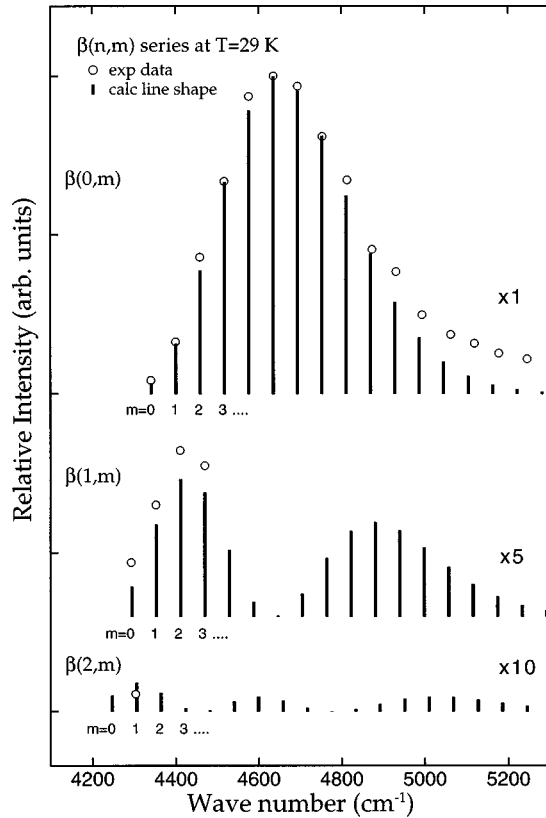


FIG. 4. Calculated relative intensity for the  $\beta(0,m)$ ,  $\beta(1,m)$ , and  $\beta(2,m)$  series at  $T=29$  K (bars) and compared to the experimental integrated intensity ( $\circ$ ). See Fig. 2 and the text for additional details.

agreement for the higher-phonon replicas is due to the difficulty of uniquely separating the experimental data for the higher-phonon replicas into contributions from the  $\beta(0,m)$  and from the  $\beta(1,m)$  series. The experimental data presented in Fig. 4 for the  $\beta(0,m)$  series higher-phonon replicas are therefore the sums of the intensities of both the  $\beta(0,m)$  and the  $\beta(1,m)$  series.

### B. Uniaxial stress

The  $\beta$ -series zero-phonon line  $\beta(0,0)$  has been studied for uniaxial stress  $F$  in the  $\langle 001 \rangle$ ,  $\langle 110 \rangle$ , and  $\langle 111 \rangle$  directions. The stress response for the corresponding lower-phonon replicas showed the same stress splitting behavior as that for the  $\beta(0,0)$  line, while the stress splitting for the higher phonon replicas remained undetected even for the highest stress due to their larger half-widths. The result for compressive stress in the  $\langle 001 \rangle$ ,  $\langle 110 \rangle$ , and  $\langle 111 \rangle$  directions is presented in Fig. 5. Stress in the  $\langle 001 \rangle$  direction results in a nonlinear shift, but no splitting of the line was detected. For stress in the  $\langle 110 \rangle$  and  $\langle 111 \rangle$  directions, the  $\beta(0,0)$  line splits into two components, which also shift with nonlinear rates. The nonlinear stress response is presumably due to stress-induced interactions with other nearby electronic states (see further below). This splitting pattern, i.e., the number of components for the different stress directions, is characteristic of transitions at a trigonal center between two nondegenerate electronic states. When the stress is applied in the  $\langle 001 \rangle$  direction, all centers will be at the same angle to the stress direction and no split-

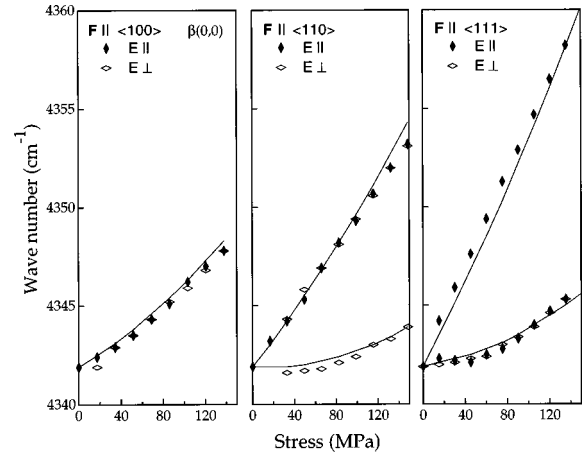


FIG. 5. Stress splitting for the  $\beta(0,0)$  line for  $F \parallel \langle 100 \rangle$ ,  $\langle 110 \rangle$ , and  $\langle 111 \rangle$ . The solid lines were obtained from a fitting procedure. See the text for details.

ting of the line is expected. However, when stress is applied in the  $\langle 110 \rangle$  and  $\langle 111 \rangle$  directions there are two nonequivalent orientations of the centers and the line should thus split into two components.

In Fig. 6 the polarization behavior for the stress split  $\beta(0,0)$  line is presented for stress in  $\langle 110 \rangle$  and  $\langle 111 \rangle$  directions. In Table I the expected linear stress-induced splittings are presented together with the expected polarization rules for a  $\pi$  dipole at a trigonal center.<sup>8</sup> The results in Fig. 6 and in Table I clearly show that the  $\beta(0,0)$  line is due transitions between two orbital singlets at a trigonal center with a transition moment oriented along the  $\langle 111 \rangle$  direction. Furthermore, this result indicates that both partners in the  $\beta(0,0)$  line are orbital singlets and that they are not due to an  $E$  doublet split by an additional lower than trigonal crystal field.

The stress shifts determined for the  $\beta(0,0)$  line are thus clearly nonlinear. This is most likely due to stress-induced interaction with another electronic state. The nonlinear stress response shifts the stress split components to higher energies than expected from the linear expressions in Table I. Since no lines are observed at energies lower than the  $\beta(0,0)$  line,

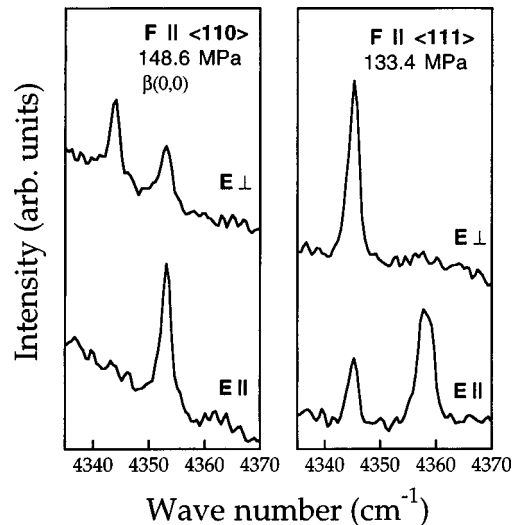


FIG. 6. Polarization spectra of the  $\beta(0,0)$  line for  $F \parallel \langle 110 \rangle$  and  $\langle 111 \rangle$ . See the text for details.

TABLE I. Energy shifts, intensity, and polarization rules in first-order perturbation theory for trigonal centers under uniaxial stress. The transitions are from a nondegenerate initial state of  $A$  ( $A_1$  or  $A_2$ ) symmetry to the final state of  $A$  symmetry, following Ref. 8.

Stress direction	Energy shifts	Intensities		
		$\mathbf{E}\parallel\mathbf{F}$	$\mathbf{E}\perp\mathbf{F}$	$\mathbf{E}\perp\mathbf{F}$
$\mathbf{F}\parallel\langle 100 \rangle$	$A_1$	4		4
$\mathbf{F}\parallel\langle 111 \rangle$	$A_1 + 2A_2$	3		0
	$A_1 - 2/3A_2$	1		4
		$\mathbf{E}\parallel\mathbf{F}$	$\mathbf{E}\perp\mathbf{F}$	$\mathbf{E}\perp\mathbf{F}$
			$\mathbf{k}\parallel\langle 001 \rangle$	$\mathbf{k}\parallel\langle 110 \rangle$
$\mathbf{F}\parallel\langle 110 \rangle$	$A_1 + A_2$	4	0	2
	$A_1 - A_2$	0	4	2

the nonlinear shift is most probably due to interactions in the initial state of the transitions. We thus have to consider the lowest initial and a yet unknown excited nearby state and their interaction under stress.

The uniaxial stress operator in  $C_{3v}$  symmetry may be written

$$\begin{aligned} \mathbf{H}_{\text{stress}} = & A_1 \text{tr}(\sigma) + A'_1(\sigma_{yz} + \sigma_{zx} + \sigma_{xy}) + E_\theta(3\sigma_{zz} - \text{tr}(\sigma)) \\ & + \sqrt{3}E_\epsilon(\sigma_{xx} - \sigma_{yy}) + E'_\theta(2\sigma_{xy} - \sigma_{yz} - \sigma_{zx}) \\ & + \sqrt{3}E'_\epsilon(\sigma_{yz} - \sigma_{zx}), \end{aligned} \quad (2)$$

where the stress tensor components  $\sigma_{ij}$  refer to the cubic axis. The two electronic operators on the first line,  $A_1$  and  $A'_1$  symmetry, whereas the other ones have  $E$  symmetry. We know from the polarization results that the lowest ground state is an orbital singlet and the  $A_1$  operators will thus only connect the ground state with states having the same symmetry. The  $E$  operators will only be active in the case in which the interacting higher-lying state has  $E$  symmetry.

Here we will study only the case for which both the interacting states are orbital singlets, which will be shown to satisfactorily account for the observed nonlinear stress shifts. We have also studied the case when the higher-lying state has  $E$  symmetry, but with limited success, i.e., a less satisfactory fit to the experimental data. Second-order perturbation theory yields two additional terms,  $B_1(\text{tr}(\sigma))^2$

+  $B_2(\sigma_{yz} + \sigma_{zx} + \sigma_{xy})^2$  that have to be added to the linear energy shifts in Table I. A least-squares fit to the experimental data was carried out and the solid lines in Fig. 5 represent the result for  $A_1 = 32.0 \text{ cm}^{-1}/\text{GPa}$ ,  $A_2 = 35.1 \text{ cm}^{-1}/\text{GPa}$ ,  $B_1 = 100 \text{ cm}^{-1}/\text{GPa}^2$ , and  $B_2 = 20 \text{ cm}^{-1}/\text{GPa}^2$ , where  $A_1$  and  $A_2$  are defined as the reduced matrix elements  $A_1 = [\Gamma_f \parallel A_1 \parallel \Gamma_i] - [\Gamma_i \parallel A_1 \parallel \Gamma_i]$  and  $A_2 = [\Gamma_f \parallel A'_1 \parallel \Gamma_f] - [\Gamma_i \parallel A'_1 \parallel \Gamma_i]$ , where  $\Gamma_i$  and  $\Gamma_f$  denote the initial and final states, respectively. A plausible candidate for the interacting electronic state is the  $\eta$ -series initial electronic state.

Recently, electronic-structure calculations were carried out for different Au-Li and Pt-Li complexes in silicon.<sup>9</sup> The complexes all contained a single substitutional transition-metal atom and thus no results were obtained for Au<sub>2</sub>-Li complexes that would be of interest here.

Several complexes that involve a transition metal and Li have been studied recently by magnetic resonance.<sup>10</sup> None of the electron paramagnetic resonance centers were assigned to a Au<sub>2</sub>-Li complex, which, at a first glance, indicates that the Au<sub>2</sub>-Li complex is not formed. However, we have carried out a Zeeman study on the Au-Li spectrum reported here, but no splittings were observed, which indicates that the center is nonparamagnetic and thus is impossible to observe by magnetic resonance.

#### IV. CONCLUSIONS

The electronic and vibrational properties of a gold- and lithium-related complex in silicon have been studied using Fourier-transform infrared spectroscopy in conjunction with uniaxial stress. The spectrum consists of three series of zero-phonon lines and several corresponding phonon replicas. Phonon energies of about 59 and 47  $\text{cm}^{-1}$  were deduced for the final and initial states of the transitions. Uniaxial stress in conjunction with polarization spectroscopy has conclusively demonstrated that the center has trigonal symmetry. The close similarity between this spectrum and those for the Au<sub>2</sub> and Au<sub>2</sub>-Fe centers leads us to tentatively identify the Au-Li center as a Au<sub>2</sub>-Li complex.

#### ACKNOWLEDGMENTS

The authors acknowledge financial support from the Swedish Natural Science Research Foundation and the Swedish Research Council for Engineering Sciences.

<sup>1</sup>G. D. Watkins, M. Kleverman, A. Thilderkvist, and H. G. Grimmeiss, Phys. Rev. Lett. **67**, 1149 (1991).

<sup>2</sup>M. Kleverman, J. Olajos, and H. G. Grimmeiss, Phys. Rev. B **35**, 4093 (1987).

<sup>3</sup>G. D. Watkins, Physica B & C **117&118**, 9 (1983).

<sup>4</sup>M. Kleverman, S. Ghatnekar Nilsson, and H. G. Grimmeiss, Phys. Rev. Lett. **67**, 1146 (1991).

<sup>5</sup>A. Thilderkvist, S. Ghatnekar Nilsson, M. Kleverman, and H. G. Grimmeiss, Phys. Rev. B **49**, 16926 (1994).

<sup>6</sup>P. Tidlund and M. Kleverman (unpublished).

<sup>7</sup>A. M. Stoneham, *Theory of Defects in Solids* (Clarendon, Oxford, 1975).

<sup>8</sup>A. A. Kaplyanskii, Opt. Spektrosk. **16**, 602 (1964).

<sup>9</sup>H. Wehrich, H. Overhof, P. Altehald, S. Grulich-Weber, and J.-M. Spaeth, Phys. Rev. B **52**, 5007 (1995).

<sup>10</sup>P. Altehald, S. Grulich-Weber, J.-M. Spaeth, H. Overhof, H. Wehrich, and M. Höhne, Phys. Rev. B **52**, 4998 (1995).